

DRIFu: Differentiable Rendering and Implicit Function-based Single-View 3D Reconstruction

Zijian Kuang¹, Lihang Ying², Shi Jin³, and Li Cheng⁴

Department of Computing Science, University of Alberta, Edmonton, Canada

Email: ¹kuang@ualberta.ca

ZeroBox Inc., Edmonton, Canada

Email: ²leo@zerobox.ai, ³shi@zerobox.ai

Department of Electrical and Computer Engineering, University of Alberta,
Edmonton, Canada

Email: ⁴lcheng5@ualberta.ca

Abstract. The Differentiable Rendering and Implicit Function-based model (DRIFu) draws its roots from the Pixel-aligned Implicit Function (PIFu), a pioneering 3D digitization technique initially designed for clothed human bodies. PIFU excels in capturing nuanced body shape variations within a low-dimensional space and has been extensively trained on human 3D scans. However, the application of PIFU to live animals poses significant challenges, primarily due to the inherent difficulty in obtaining the cooperation of animals for 3D scanning. In response to this challenge, we introduce the DRIFu model, specifically tailored for animal digitization. To train DRIFu, we employ a curated set of synthetic 3D animal models, encompassing diverse shapes, sizes, and even accounting for variations such as baby birds. Our innovative alignment tools play a pivotal role in mapping these diverse synthetic animal models onto a unified template, facilitating precise predictions of animal shape and texture. Crucially, our template alignment strategy establishes a shared shape space, allowing for the seamless sampling of new animal shapes, posing them realistically, animating them, and aligning them with real-world data. This groundbreaking approach revolutionizes our capacity to comprehensively understand and represent avian forms. For further details and access to the project, the project website can be found at <https://github.com/kuangzijian/drifu-for-animals>.

Keywords: 3D reconstruction from single view, 3D digitization, Differentiable rendering, implicit function, Unsupervised Learning

1 Introduction

The exploration of animal detection, tracking, and behavior analysis is crucial across various fields like biology, ecology, farming, and entertainment. Despite its broad applications, the computer vision community has primarily focused on human modeling and behavior analysis.

However, acquiring 3D data for training models is exceptionally challenging. Models like PIFu [1] and SMPL [2] rely on extensive databases with thousands

of 3D scans, covering diverse human shapes and poses. Humans, as cooperative subjects, facilitate this process. Unfortunately, bringing numerous wild animals into a controlled lab for scanning is impractical, and taking scanning equipment into the wilderness is logistically complex.

To address this challenge, we propose a two-stage model that combines Differentiable Rendering and Implicit representation. This innovative model leverages a two-stage approach to learn from synthetic animal 3D models and enhance its capabilities by generating additional 3D models from single-view images of real animals. In Stage 1, the process involves utilizing a pixel-aligned implicit function to predict the continuous inside/outside probability field of a synthetic bird based on the provided image. Employing sophisticated differentiable rendering techniques, a render is created for the 3D implicit representation of the synthetic bird generated by a pixel-aligned feature decoder. This rendered output is then transformed into 2D images, facilitating multi-view self-supervised learning.

Moving to Stage 2, the model makes use of the pixel-aligned feature encoder-decoder, which has been pre-trained on synthetic birds. Transfer learning is employed by integrating real bird images along with their silhouettes, enhancing the model’s ability to generalize to real-world scenarios. This two-stage strategy ensures a robust and versatile approach to animal 3D model generation, where synthetic data aids in the learning process and real-world images contribute to the model’s adaptability and practical utility.

Our experiment primarily focuses on the 3D digitalization of birds. In Stage 1, we collected 20 synthetic 3D bird models encompassing various bird types, such as owls, blue jays, toucans, parrots, ducks, and pigeons, to train our model. For Stage 2, we employed 5964 unseen real bird images along with their silhouettes for additional model training. Our results demonstrate that our differentiable rendering and implicit function-based approach outperform state-of-the-art methods [3, 4] in both quantitative and qualitative aspects of bird 3D digitalization. Moreover, we extended our method to other animals, including horses, cows, bears, and dogs, with qualitative results presented in this paper.

2 Related Work

2.1 3D Shape Representation

Various representations have been explored in the context of 3D processing tasks, encompassing diverse modalities such as point clouds [5], implicit surfaces [6, 7], triangular meshes [3, 8–13], and voxel grids [14–21]. Although both voxels and triangular meshes lend themselves well to deep learning architectures (e.g., VON [22, 23], PointNet [24, 25], etc.), they grapple with issues of memory inefficiency or lack suitability for differentiable rendering. Consequently, in this undertaking, we opt for point clouds [3, 8–13] as our preferred representation for 3D reconstruction.

2.2 Single-view 3D Reconstruction

The objective of single-view 3D reconstruction [1, 5, 14–20, 26] is to reconstruct a three-dimensional shape given a solitary input image. This challenging task has been approached by various methods with different degrees of supervision. Some approaches [11–13] rely on image and ground truth 3D mesh pairs as supervision, necessitating extensive manual annotation efforts [27] or being constrained to synthetic data [28]. More recent endeavors [8–10, 29] sidestep the need for 3D supervision by leveraging differentiable renderers [8, 9, 29] and the "analysis-by-synthesis" approach, either with multiple views or known ground truth camera poses. In a bid to relax constraints on supervision, Kanazawa et al. [3] explored 3D reconstruction from a collection of images of different instances. Nevertheless, their method still requires annotated 2D keypoints to accurately infer camera pose. This work is also notable for being the first to propose a learnable category-level 3D template shape, albeit one that needs initialization from a keypoint-dependent 3D convex hull. Similar problem settings have been explored in other methods [30–32], but with object categories limited to rigid or structured objects, such as cars or faces. Diverging from these approaches, our focus encompasses both rigid and non-rigid objects (e.g., birds, horses, penguins, motorbikes, and cars). We present a method that jointly estimates a 3D shape, and texture, from a single-view image, relying on synthetic animals' 3D template and collection of real animal images with silhouettes as supervisions. In essence, we eliminate the need for real animals' 3D template priors, annotated key points, or multi-view real animal images.

3 Approach

To achieve a comprehensive reconstruction of the 3D mesh for an object instance from an image, a network must possess the capability to simultaneously predict the shape and texture of the object, along with the camera pose of the image. In pursuit of this goal, we initiate our efforts with the pre-existing network introduced in [1] (PIFU) as the foundational reconstruction network. Our objective, when presented with either single or multi-view images, is to reconstruct the underlying 3D geometry and texture of an animal while retaining the intricacies depicted in the images as shown in Figure. 1.

Similar to PIFU, we utilize Pixel-Aligned Implicit Functions (PIFu), a spatially-aligned and memory-efficient 3D representation for surfaces. Implicit functions characterize a surface as the level set of a function, denoted as $f(X) = 0$. This leads to an efficient memory representation where the embedding space of the surface doesn't require explicit storage. The proposed pixel-aligned implicit function comprises a fully convolutional image encoder g and a continuous implicit function f , represented by multi-layer perceptrons (MLPs). The surface is defined as a level set of this function.

$$f(F(x), z(X)) = s : s \in \mathbb{R} \quad (1)$$

For a 3D point X , where $x = \pi(X)$ is its 2D projection and $z(X)$ is the depth in camera coordinates, $F(x) = g(I(x))$ is the image feature at x . Assuming a weak-perspective camera (extendable to perspective cameras), note that we use bilinear sampling for continuous 2D projection. The key is learning an implicit function over 3D space with pixel-aligned image features, preserving local image details. The implicit function’s continuous nature enables detailed geometry generation with arbitrary topology efficiently and can extend to various domains like RGB colors.

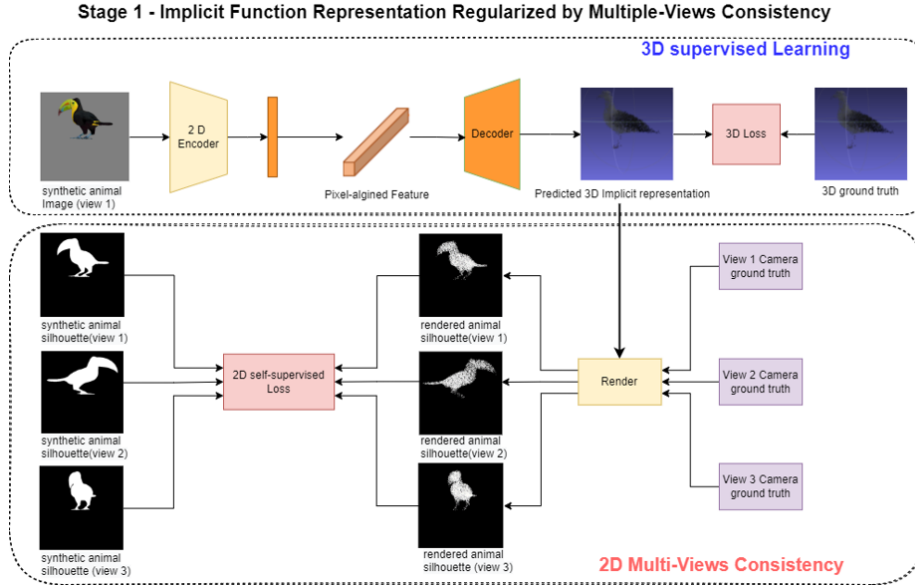


Fig. 1: An overview of our differentiable rendering and implicit function-based model digitalization pipeline. In Stage 1, we use a pixel-aligned implicit function to predict the continuous inside/outside probability field [1] of the synthetic bird from the given bird image. Then, employing differentiable rendering techniques, we create a render for the 3D implicit representation of the synthetic bird generated by a pixel-aligned feature decoder, rendering it into 2D images for multi-view self-supervised learning.

3.1 3D supervised learning from single view image

To reconstruct the 3D implicit representation, we represent the ground truth surface as a 0.5 level-set of a continuous 3D occupancy field:

$$f_v^*(X) = \begin{cases} 1, & \text{if } X \text{ is inside mesh surface} \\ 0, & \text{otherwise} \end{cases}. \quad (2)$$

We train a pixel-aligned implicit function f_v by minimizing the average mean squared error between the predicted 3D point cloud against the ground truth 3D point cloud:

$$\mathcal{L}_V = \frac{1}{n} \sum_{i=1}^n |f_v(F_V(x_i), z(X_i)) - f_v^*(X_i)|^2 \quad (3)$$

where $X_i \in \mathbb{R}^3$, $F_V(x) = g(I(x))$ is the image feature from the image encoder g at $x = \pi(X)$, and n is the number of sampled points. Given a pair of an input image and the corresponding 3D mesh that is spatially aligned with the input image, the parameters of the image encoder g and the implicit function f_v are jointly updated by minimizing Eq. 3. As Bansal et al. [33] demonstrate for semantic segmentation, training an image encoder with a subset of pixels does not hurt convergence compared with training with all the pixels. During inference, we densely sample the probability field over the 3D space and extract the iso-surface of the probability field at threshold 0.5 using the Marching Cube algorithm [34]. This implicit surface representation is suitable for detailed objects with arbitrary topology.

While texture inference is typically executed on either a 2D surface parameterization [3, 35] or in view-space [36], PIFu allows us to directly predict RGB colors on the surface geometry by defining s in Eq. 1 as an RGB vector field instead of a scalar field. This facilitates the texturing of shapes with arbitrary topology and self-occlusion. However, extending PIFu to color prediction is a challenging task since RGB colors are defined only on the surface, whereas the 3D occupancy field is defined over the entire 3D space. In this context, we emphasize the modifications made to PIFu in terms of training procedures and network architecture.

Given sampled 3D points on the surface $X \in \Omega$, the objective function for texture inference is the average of the L1 error of the sampled colors as follows:

$$\mathcal{L}_C = \frac{1}{n} \sum_{i=1}^n |f_c(F_C(x_i), z(X_i)) - C(X_i)| \quad (4)$$

where $C(X_i)$ is the ground truth RGB value on the surface point $X_i \in \Omega$, and n is the number of sampled points. We observed that training f_c with the above loss function directly leads to severe overfitting. The challenge arises because f_c is expected to learn not only the RGB color on the surface but also the underlying 3D surfaces of the object. This is crucial for f_c to infer the texture of unseen surfaces with different poses and shapes during inference, posing a significant challenge.

To address this issue, we introduce the following modifications. First, we condition the image encoder for texture inference with the image features learned for surface reconstruction, denoted as F_V . This enables the image encoder to focus on color inference for a given geometry, even when unseen objects have different shapes, poses, or topologies. Additionally, we introduce an offset $\epsilon \sim \mathcal{N}(0, d)$ to the surface points along the surface normal N , allowing the color to

be defined not only on the exact surface but also in the 3D space around it. With these modifications, the training objective function can be rewritten as:

$$\mathcal{L}_C = \frac{1}{n} \sum_{i=1}^n |f_c(F_C(x'_i, F_V), X'_{i,z}) - C(X_i)|, \quad (5)$$

where $X_{0i} = X_i + \epsilon \cdot N_i$. We set $d = 1.0$ cm for all experiments. For details regarding the network architecture for texture inference, please refer to the supplemental material.

To further leverage the 3D information, we devised a 2D multi-view consistency strategy as shown in Figure. 1.

3.2 2D multi-view consistency

The envisioned 3D implicit representation should manifest uniformity when viewed from different angles. In pursuit of this, we implemented a 2D multi-view consistency strategy, harnessing the capabilities of differentiable rendering techniques as shown in Figure. 1. This methodology guarantees that the pixel-level implicit function acquires supplementary insights from synthetic animal 3D models. Through the application of a render function $R(P)$, where P signifies the predicted point cloud 3D implicit representation, the model generates three distinct views I_v by adjusting camera parameters. This process enables 2D self-supervised learning via MSE loss, specifically on the rendered 2D views.

$$\mathcal{L}_M = \frac{1}{n} \sum_{i=1}^n (I_{vi} - \hat{I}_{gi})^2 \quad (6)$$

During training, We opted for a point cloud as the 3D implicit representation instead of marching cubes, primarily due to the non-differentiable nature of the marching cubes algorithm, which poses challenges in gradient-based optimization during inference.

Traditional Marching Cubes, as originally proposed, is not differentiable. The algorithm is a geometric method used for surface reconstruction and visualization of isosurfaces from 3D scalar fields. It involves thresholding the scalar field to create a binary mask, and then constructing polygonal surfaces based on the intersections of this mask with a grid of cubes.

For differentiable rendering or applications where gradients are needed for optimization (like in training neural networks), differentiable versions of Marching Cubes or similar algorithms are used. These versions incorporate smooth approximations and can allow for gradient-based optimization techniques.

Differentiable rendering is an active area of research, and various techniques are employed to make traditionally non-differentiable operations, like surface reconstruction with Marching Cubes, differentiable for use in gradient-based optimization, particularly for applications in neural network training.

Utilizing differentiable rendering methods, we generate a render for the 3D implicit representation of the synthetic bird produced by a pixel-aligned feature

decoder. Three fixed camera views (0 degrees, 90 degrees, and 180 degrees) are configured for the renderer, and the point cloud 3D representation is then rendered into these static views for self-supervised learning.

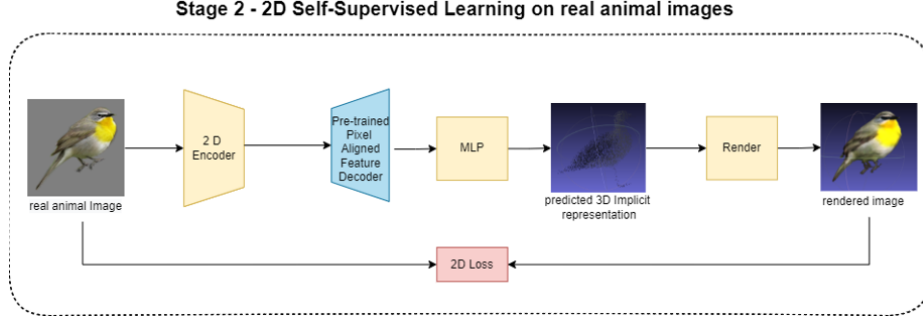


Fig. 2: In Stage 2, we utilize the pixel-aligned feature encoder decoder that is pre-trained on synthetic birds. We apply transfer learning by incorporating real bird images along with their silhouettes.

3.3 2D self-supervised learning on real animal images

In the second stage, we harness the implicit function pre-trained on synthetic animal images and employ real animal images to fine-tune the function using a self-supervised learning approach as shown in Figure. 2. Initially, the implicit function generates a 3D representation, which is then rendered into a 2D image using the render function $R(P)$. Subsequently, a 2D loss function is applied for comparison. During the inference phase, the trained implicit function can be directly applied to a given 2D animal image falling within the classes trained in both stages (in this instance, birds).

4 Experiments

We assess our proposed methodology across diverse datasets, encompassing bird images from the CUB-200-2011 dataset [37] and images of horses, zebras, and cows from the ImageNet dataset [38], which features a broad array of various animal species.

4.1 Implementation Detail

Like PIFU [1], our texture inference image encoder adopts the CycleGAN architecture [39], incorporating residual blocks [40]. The implicit function is built on a multi-layer perceptron with layers featuring skip connections from the image feature $F(x)$ and depth z , inspired by [41], for effective depth information

propagation. The refined implicit function in stage 2 incorporates an additional multi-layer perceptron to further enhance the network with real animal images.

The Differentiable rendering method we used is PyTorch3D [42], which provides the method for rasterizing a batch of pointclouds.

During stage 1, we conducted training for 100 epochs for both the 3D implicit function network and the 2D render network with a learning rate of 0.001. In stage 2, we proceeded with another 50 epochs of training for the refined implicit function network, adjusting the learning rate to 0.0005.

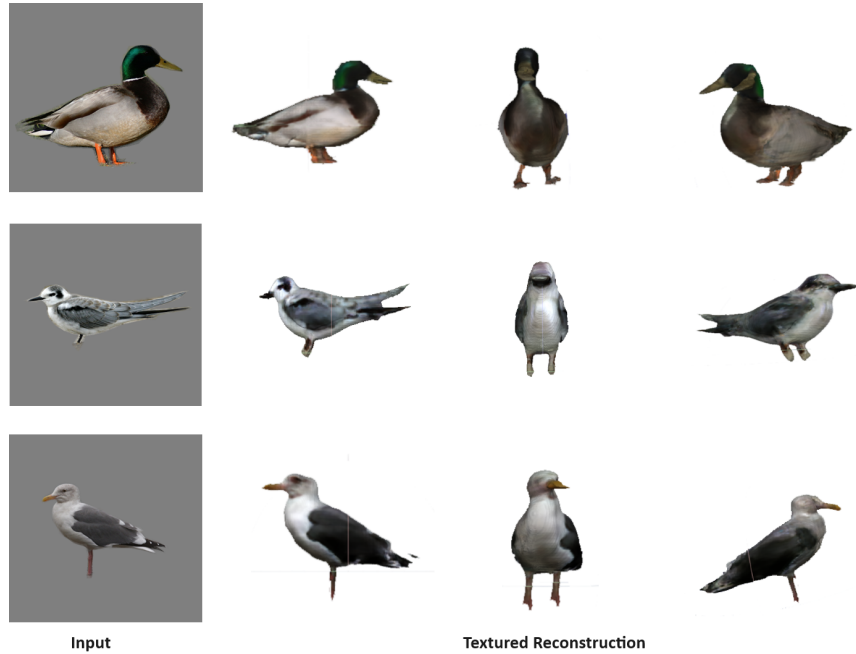


Fig. 3: Qualitative single-view 3D and textured reconstruction results on real bird images from CUB-200-2011 dataset [37].

4.2 Qualitative Results

We present the acquired 3D representations for both birds and horses in Figure. 3, Figure. 4 and Figure. 5, encapsulating the distinctive shape features of each category. Notably, our results excel in horse prediction, surpassing CMR and UMR by capturing more intricate details like the legs and tail of the horse. The visualizations vividly showcase the accuracy and detailed representation achieved by our model.

In Figure. 3, we showcase the outcomes of our digitization process using actual bird images sourced from the CUB-200-2011 dataset [37]. Our DRIFu proves its adaptability across a diverse range of bird species. The method excels

in generating high-resolution local details and inferring plausible 3D surfaces, even in unseen regions. Additionally, it successfully infers complete textures from a single input image, enabling a comprehensive view of our 3D models from all angles.

Much like shape evaluation, texture assessment is computed between the rendered and ground truth 2D images, employing precision and recall to gauge the outcomes. Our approach outperforms the other models as well.

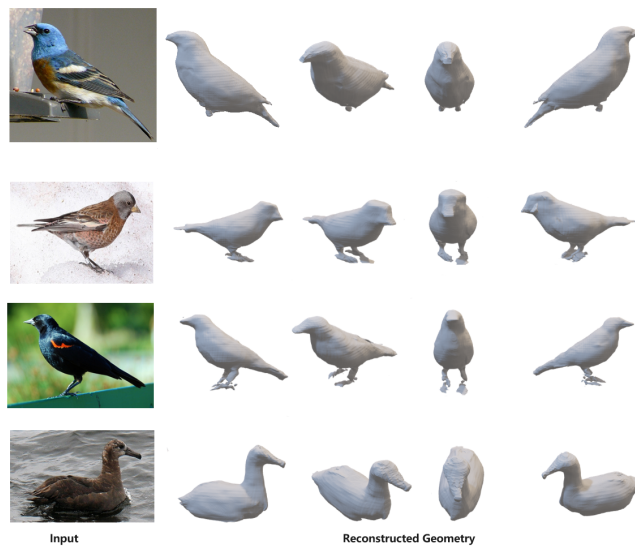


Fig. 4: More qualitative single-view 3D reconstruction results on real bird images from CUB-200-2011 dataset [37]

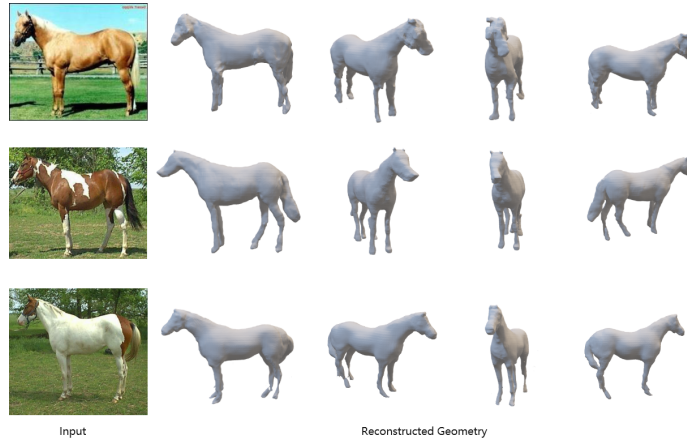


Fig. 5: More qualitative single-view 3D reconstruction results on real animal images from Weizmann horses dataset [43].

4.3 Quantitative Results

We quantitatively evaluate our reconstruction accuracy with three metrics in terms of 2D shape, and texture. However, a lack of ground truth for 3D meshes or camera poses in these datasets hinders a quantitative evaluation in 3D.

We initially assess shape reconstruction for birds. Given the absence of ground truth 3D shapes in the CUB-200-2011 dataset [37], we adhere to [3] and calculate mask reprojection accuracy, represented by the intersection over union (IoU) between rendered and ground truth silhouettes. Table. 1 illustrates that our model surpasses other state-of-the-art single-view bird 3D reconstruction models, showcasing its capability to predict 3D mesh reconstructions that align well with 2D observations.

Much like shape evaluation, texture assessment is computed between the rendered and ground truth 2D images, employing precision and recall to gauge the outcomes. Our approach outperforms the other models as well.

Table 1: Quatitative evaluation of mask IoU and texture precision and recall on CUB-200-2011 dataset [37]. The comparisons are against the baseline supervised models [3, 4].

Methods	MaskIoU	Texture Precision	Texture Recall
CMR [3]	0.706	0.652	0.612
UMR [4]	0.734	0.701	0.54
Ours	0.836	0.837	0.721

We conducted additional evaluations comparing our model to the baseline supervised models [3, 4] using real horse images from the Weizmann Horses dataset [43]. The results of the evaluation are presented in Table. 2. The use of implicit representation enables us to achieve higher fidelity.

Table 2: Quatitative evaluation of mask IoU and texture precision and recall on weizmann Horses dataset [43]. The comparisons are against the baseline supervised models [3, 4].

Methods	MaskIoU	Texture Precision	Texture Recall
CMR [3]	0.606	0.552	0.423
UMR [4]	0.534	0.601	0.54
Ours	0.765	0.801	0.721

5 Conclusion

This research aims to pioneer a model for the intricate task of reconstructing the 3D shape and texture of animals using single-view images of real animals. A distinctive feature of our approach is the utilization of specific synthetic animal 3D models for supervision, enabling the model to learn from a controlled and diverse set of virtual animal instances. The crux of our methodology lies in the introduction of a self-supervised differentiable rendering framework, carefully designed to enforce multi-view consistency between the reconstructed 3D representations and the corresponding images. This strategic approach markedly reduces ambiguities in the simultaneous prediction of 3D shape and texture from 2D observations.

Additionally, we integrate a transfer learning-based self-supervised framework, extending the capabilities of our model to leverage the learned 3D representation when confronted with unseen real animal images. This transfer learning mechanism enhances the adaptability and robustness of our model to diverse real-world scenarios.

The efficacy of our proposed method is substantiated through extensive experimental results. Notably, our approach surpasses the performance of state-of-the-art supervised category-specific reconstruction techniques. The experimental outcomes underscore the potential and versatility of our model in advancing the field of 3D shape and texture reconstruction from single-view images, particularly in the domain of real animals.

References

1. S. Saito, Z. Huang, R. Natsume, S. Morishima, A. Kanazawa, and H. Li, “Pifu: Pixel-aligned implicit function for high-resolution clothed human digitization,” 2019.

2. M. Loper, N. Mahmood, J. Romero, G. Pons-Moll, and M. J. Black, "SMPL: A skinned multi-person linear model," pp. 248:1–248:16, Oct. 2015.
3. A. Kanazawa, S. Tulsiani, A. A. Efros, and J. Malik, "Learning category-specific mesh reconstruction from image collections," 2018.
4. Li, Xueting, S. Liu, K. Kim, S. De Mello, V. Jampani, M.-H. Yang, and J. Kautz, "Self-supervised single-view 3d reconstruction via semantic consistency," 2020.
5. H. Fan, H. Su, and L. Guibas, "A point set generation network for 3d object reconstruction from a single image," 2016.
6. S. Liu, S. Saito, W. Chen, and H. Li, "Learning to infer implicit surfaces without 3d supervision," 2019.
7. L. Mescheder, M. Oechsle, M. Niemeyer, S. Nowozin, and A. Geiger, "Occupancy networks: Learning 3d reconstruction in function space," 2019.
8. H. Kato, Y. Ushiku, and T. Harada, "Neural 3d mesh renderer," 2017.
9. S. Liu, T. Li, W. Chen, and H. Li, "Soft rasterizer: A differentiable renderer for image-based 3d reasoning," 2019.
10. H. Kato and T. Harada, "Learning view priors for single-view 3d reconstruction," 2019.
11. N. Wang, Y. Zhang, Z. Li, Y. Fu, W. Liu, and Y.-G. Jiang, "Pixel2mesh: Generating 3d mesh models from single rgb images," 2018.
12. J. Pan, X. Han, W. Chen, J. Tang, and K. Jia, "Deep mesh reconstruction from single rgb images via topology modification networks," 2019.
13. C. Wen, Y. Zhang, Z. Li, and Y. Fu, "Pixel2mesh++: Multi-view 3d mesh generation via deformation," 2019.
14. C. B. Choy, D. Xu, J. Gwak, K. Chen, and S. Savarese, "3d-r2n2: A unified approach for single and multi-view 3d object reconstruction," 2016.
15. R. Girdhar, D. F. Fouhey, M. Rodriguez, and A. Gupta, "Learning a predictable and generative vector representation for objects," 2016.
16. J. Gwak, C. B. Choy, A. Garg, M. Chandraker, and S. Savarese, "Weakly supervised 3d reconstruction with adversarial constraint," 2017.
17. S. Tulsiani, T. Zhou, A. A. Efros, and J. Malik, "Multi-view supervision for single-view reconstruction via differentiable ray consistency," 2017.
18. O. Wiles and A. Zisserman, "Silnet : Single- and multi-view reconstruction by learning from silhouettes," 2017.
19. X. Yan, J. Yang, E. Yumer, Y. Guo, and H. Lee, "Perspective transformer nets: Learning single-view 3d object reconstruction without 3d supervision," 2017.
20. R. Zhu, H. K. Galoogahi, C. Wang, and S. Lucey, "Rethinking reprojection: Closing the loop for pose-aware shapereconstruction from a single image," 2017.
21. C. Häne, S. Tulsiani, and J. Malik, "Hierarchical surface prediction for 3d object reconstruction," 2017.
22. J. Wu, C. Zhang, T. Xue, W. T. Freeman, and J. B. Tenenbaum, "Learning a probabilistic latent space of object shapes via 3d generative-adversarial modeling," 2017.
23. J.-Y. Zhu, Z. Zhang, C. Zhang, J. Wu, A. Torralba, J. B. Tenenbaum, and W. T. Freeman, "Visual object networks: Image generation with disentangled 3d representation," 2018.
24. C. R. Qi, H. Su, K. Mo, and L. J. Guibas, "Pointnet: Deep learning on point sets for 3d classification and segmentation," 2017.
25. C. R. Qi, L. Yi, H. Su, and L. J. Guibas, "Pointnet++: Deep hierarchical feature learning on point sets in a metric space," 2017.
26. P. Henderson and V. Ferrari, "Learning to generate and reconstruct 3d meshes with only 2d supervision," 2018.

27. Y. Xiang, W. Kim, W. Chen, J. Ji, C. Choy, H. Su, R. Mottaghi, L. Guibas, and S. Savarese, "Objectnet3d: A large scale database for 3d object recognition," 2016.
28. A. X. Chang, T. Funkhouser, L. Guibas, P. Hanrahan, Q. Huang, Z. Li, S. Savarese, M. Savva, S. Song, H. Su, J. Xiao, L. Yi, and F. Yu, "Shapenet: An information-rich 3d model repository," 2015.
29. W. Chen, J. Gao, H. Ling, E. J. Smith, J. Lehtinen, A. Jacobson, and S. Fidler, "Learning to predict 3d objects with an interpolation-based differentiable renderer," 2019.
30. A. Szabó and P. Favaro, "Unsupervised 3d shape learning from image collections in the wild," 2018.
31. S. Wu, C. Rupprecht, and A. Vedaldi, "Photo-geometric autoencoding to learn 3d objects from unlabelled images," 2019.
32. P. Henderson and V. Ferrari, "Learning single-image 3d reconstruction by generative modelling of shape, pose and shading," 2019.
33. A. Bansal, X. Chen, B. Russell, A. Gupta, and D. Ramanan, "Pixelnet: Representation of the pixels, by the pixels, and for the pixels," 2017.
34. W. E. Lorensen and H. E. Cline, "Marching cubes: A high resolution 3d surface construction algorithm," New York, NY, USA, 1987. [Online]. Available: <https://doi.org/10.1145/37402.37422>
35. R. A. Güler, N. Neverova, and I. Kokkinos, "Densepose: Dense human pose estimation in the wild," 2018.
36. R. Natsume, S. Saito, Z. Huang, W. Chen, C. Ma, H. Li, and S. Morishima, "Siclope: Silhouette-based clothed people," 2019.
37. S. B. Wah, Catherine, "The caltech-ucsd birds-200-2011 dataset," 2011.
38. J. Deng, W. Dong, R. Socher, L.-J. Li, K. Li, and L. Fei-Fei, "Imagenet: A large-scale hierarchical image database," 2009.
39. J.-Y. Zhu, T. Park, P. Isola, and A. A. Efros, "Unpaired image-to-image translation using cycle-consistent adversarial networks," 2020.
40. J. Johnson, A. Alahi, and L. Fei-Fei, "Perceptual losses for real-time style transfer and super-resolution," 2016.
41. Z. Chen and H. Zhang, "Learning implicit fields for generative shape modeling," 2019.
42. N. Ravi, J. Reizenstein, D. Novotny, T. Gordon, W.-Y. Lo, J. Johnson, and G. Gkioxari, "Accelerating 3d deep learning with pytorch3d," 2020.
43. E. Borenstein, "Weizmann horse database," 2011.